Induced Far-Infrared Absorption in Mixed Alkali-Halide Crystals

de Jong, C.; Wegdam, G.H.; van der Elsken, J.

Published in:
Physical Review. B, Condensed Matter

PHYSICAL REVIEW B VOLUME 8, NUMBER 10 15 NOVEMBER 1973

Induced Far-Infrared Absorption in Mixed Alkali Halide Crystals

C. de Jong, G. H. Wegdam, and J. van der Elsken
Laboratory for Physical Chemistry, University of Amsterdam, The Netherlands
(Received 17 August 1972; revised manuscript received 17 July 1973)

The results are presented of far-infrared-absorption measurements of potassium iodide single crystals containing rubidium iodide in concentrations up to 10 mole %. At very low impurity concentrations a gap mode is found in the phonon gap of KI. When the concentration of RbI is raised, the gap mode becomes a very strong band and a spectrum emerges in the acoustic-phonon region. Comparison of theory with experiment is achieved by calculating a simulated absorption spectrum. Use is made of the phonon eigendata of the host crystal and of a model for the impurity in its surroundings which includes the elastic relaxation of the lattice around the impurity. The absorption coefficient is expressed in terms of displacement-displacement Green's functions, and the Green's functions are developed in a Taylor series in the impurity concentration. The evaluation of the first- and second-order coefficients of the series through a diagram technique is discussed. The experimentally determined acoustic spectrum of the KI:RbI crystals agrees very well with the simulated spectra involving first- and second-order terms.

I. INTRODUCTION

Much attention has been paid in the past decades to crystalline systems containing impurities. In the experimental field infrared spectroscopy has played a major role. The measured phenomena fall into three groups: (a) local and gap modes of isolated impurities which are found with a large number of impurities mainly in alkali halides,[1-4] (b) induced infrared activity of the phonon spectrum of the host by impurities,[5] and (c) spectra of crystals containing a considerable amount of impurities or mixed crystals.[6-9]

On the theoretical side, progress has been made by using powerful mathematical tools. Any model calculation tends to become lengthy and intricate because the impure system lacks the translational symmetry of the pure crystal. Local and gap modes can be dealt with by perturbation theory using a harmonic approximation. To describe the induced intensities in resonance modes, especially those below 20 cm^{-1}, it is necessary to take into account the anharmonicity of the lattice vibrations.[10] In calculations on crystals with high concentrations of impurities, perturbation theory with a pure crystal as the zeroth-order problem fails because the perturbation series diverges. A better approach might be to start from experimental results obtained with systems with low impurity concentrations, give a sound theoretical description of these results, and then repeat the experiments while increasing the concentration of impurities in the system. The transition from the detailed impurity spectrum to the broad mixed-crystal features can then be studied. In the theory the quantities of interest may be developed as a power series of the impurity concentration, which means physically that we assume these quantities to be built up from contributions of single impurities, impurity pairs, triplets etc.

In accordance with this approach we studied the far-infrared spectrum of potassium iodide containing rubidium impurities. The experimental results can be compared with absorption spectrum simulations calculated with an appropriate model for the impurities in the host crystal.

II. EXPERIMENTAL

The infrared absorption spectra of KI single crystals with varying Rb^+ impurity concentration were measured in the wave-number range 15–100 cm^{-1}. Use was made of a Beckmann-RIIC FS 720 interferometer; the Fourier transforms of the interferograms were obtained using a method outlined by Cooley and Tukey.[11]

The crystals were grown from the melt by the Kryopoulos technique. As a seed crystal we used a small part of the crystal containing the next lower amount of Rb. The concentration of Rb^+ ions in the samples was measured by flame photometric analysis. Samples could be prepared without difficulty with Rb^+ concentrations up to 10 mole%. All measurements were made in a liquid-helium cryostat. A conduction variable-temperature cryostat was used to investigate the temperature dependence of the spectra between 5 and 20 K. Most measurements, however, were made on samples held in an immersion cryostat at 4.2 K.

KI:Rb^+ samples containing less than 1-mole% Rb^+ ions show a gap mode which appears to be a doublet on improving the spectral resolution (see Fig. 1). Comparison with the spectrum obtained when KI is doped with 99%-pure ^{85}Rb, also shown in Fig. 1, makes it clear that a peak centered around 86.17 ± 0.05 cm^{-1} must be assigned to the $^{87}Rb^+$ gap mode and one around 86.83 ± 0.05 cm^{-1} to the $^{85}Rb^+$ gap mode. The ratio between the two surfaces is about 1:3, in good agreement with the natural abundance, 28% ^{87}Rb and 72% ^{85}Rb. A

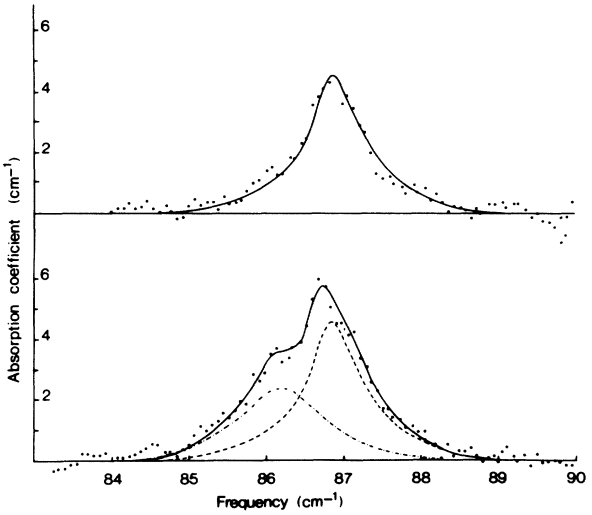

FIG. 1. Gap modes of KI:Rb^+. The upper part of the figure shows the absorption in the gap of KI doped with ^{85}Rb isotope. The lower part shows the absorption of KI doped with Rb isotopes in natural abundance (solid line). The dotted curve is a copy of the upper part and the dash-dot curve is obtained by subtraction.

previous assignment[12] of this doublet as arising from OH impurities must therefore be discarded. The total integrated absorption coefficient appears to be a linear function of the impurity concentration, approaching zero with vanishing concentration. These samples show no infrared absorption below the gap of KI in the region between 15 and 70 cm^{-1}. Furthermore, no temperature effect on the gap mode absorptions could be found between 5 and 20 K.

KI:Rb^+ samples with higher impurity concentrations up to 10-mole% Rb^+ were investigated in the same frequency region. Around 86 cm^{-1} the gap mode band becomes so strong that intensity measurements become impossible. In the acoustic region a broad absorption spectrum emerges, having features in common with the phonon density of states of KI. Such a spectrum is shown in Fig. 2. A plot of the integrated absorption coefficient A for this acoustic spectrum versus the mole fraction of Rb^+ is given in Fig. 3. There is a slight but significant deviation from linearity, enough to conclude that A is not a simple linear function of x, nor is it a function in only one power of x.

III. THEORY

Linear response theory gives the relation between the dielectric susceptibility tensor and the Fourier-transformed Green's function[13–15]:

$$\chi_{\alpha\beta}(\omega) = (1/kT)\, G(M_\beta, M_\alpha, \omega). \tag{1}$$

M_β and M_α denote components of the dipole moment. The dipole moment can be developed in a series of particle displacements or phonon displacements. Since, furthermore, the absorption coefficient is related to the susceptibility by

$$\sigma(\omega) = (4\pi\omega/nc)\,\chi''(\omega),$$

one obtains

$$\sigma(\omega) = \frac{4\pi\omega}{nckT}\,\frac{N\hbar e_{TO}^2}{2\omega_{TO}\mu V}\,\mathrm{Im}G(B_{TO}B_{TO},\omega), \tag{2}$$

where e_{TO} is the effective charge of an ion in the crystal when vibrating in the transverse-optic mode, μ is the reduced mass of positive or negative ion, B is the displacement operator of the phonon, and the other symbols have their usual meaning.

In order to find the Green's function it is necessary to construct the Hamiltonian of the system including the perturbation terms. We shall consider only the perturbation terms arising from the introduction of impurities and omit the contribution of higher-order terms in the potential energy. This contribution would have a negligible effect on the Green's function at low temperatures, and we will compare theoretical results with low-temperature

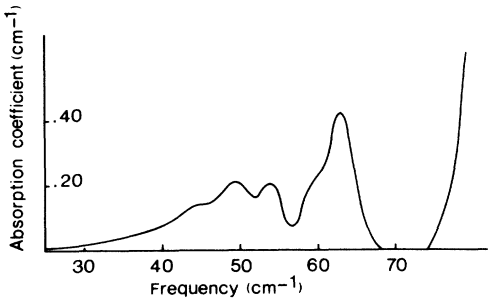

FIG. 2. Absorption spectrum of KI containing 1-mole% Rb^+. Sample thickness 0.52 cm, resolution 1.2 cm^{-1}.

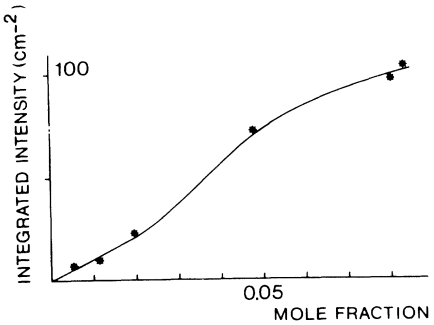

FIG. 3. Integrated infrared intensity (in units of cm^{-2}) of the activated acoustic spectrum vs the mole fraction of Rb impurities.

(4.2 K) experiments only.

We will start by considering the effect of only one impurity. This will introduce a different mass at a lattice site with unit cell label $l=s$ and atom label $k=0$, so we will find a kinetic-energy difference

$$T(1)=-\frac{\hbar^2}{2}\left(\frac{1}{M'}-\frac{1}{M_0}\right)\sum_{\alpha}\frac{\partial^2}{\partial^2 u_\alpha(s0)}\ ; \tag{3}$$

coordinate transformation into q space leads to

$$T(1)=\frac{\hbar}{4N}\left(\frac{M_0}{M'}-1\right)\sum_{qj}\sum_{q'j'}[\omega(\vec{q}j)\,\omega(\vec{q}'j')]^{1/2}\times T(\vec{q}j,\vec{q}'j')P^\dagger(\vec{q}j)P(\vec{q}'j'), \tag{4}$$

where

$$T(qj,q'j')=\sum_{\alpha} w_\alpha^*(0\,|\vec{q}j)\,w_\alpha(0\,|\vec{q}'j')\times e^{i(\vec{q}'-\vec{q})\cdot\vec{r}(s)}. \tag{5}$$

It is apparent that the perturbation contains two-phonon momentum operators. Furthermore it is clear that the perturbations caused by introducing more impurities simply add, because each kinetic-energy term contains one lattice site only.

The change in the potential energy upon introduction of impurities can likewise be expressed:

$$V(1)=\frac{\hbar}{4N}\sum_{qj}\sum_{q'j'}[\omega(\vec{q}j)\,\omega(\vec{q}'j')]^{1/2}\times D(\vec{q}j,\vec{q}'j')e^{i(\vec{q}'-\vec{q})\cdot\vec{r}(s)}\times B^\dagger(\vec{q}j)B(\vec{q}'j'); \tag{6}$$

$B(\vec{q}j)\equiv b(\vec{q}j)+b^\dagger(-\vec{q}j)$ is the phonon displacement operator and

$$D(\vec{q}j,\vec{q}'j')=\sum_{lka}\sum_{l'k'b} w_\alpha^*(k\,|\vec{q}j)e^{-i\vec{q}\cdot\vec{r}(lk)}\times\Delta\Phi_{\alpha\infty}\begin{pmatrix} s+l & s+l' \\ k & k'\end{pmatrix}(M_kM_{k'})^{-1/2}\times e^{i\vec{q}'\cdot\vec{r}(l'k')}w_\beta(k'\,|\vec{q}'j'), \tag{7}$$

which is independent of the impurity position s. The contributions of more impurities add, provided that the subspaces of the impurities do not overlap. When the impurities are neighbors or next nearest neighbors the force constants will be slightly affected. Nevertheless we will here assume additivity of the perturbation terms.

We can now proceed from the Hamiltonian to the displacement-displacement Green's function. We develop the Green's function as a series of the impurity concentration[16]

$$G=g+\frac{\partial G}{\partial x}\bigg|_{x=0}x+\frac{1}{2}\frac{\partial^2 G}{\partial x^2}\bigg|_{x=0}x^2+\cdots, \tag{8}$$

where g is the Green's function for the pure crystal,

$$\frac{\partial G}{\partial x}\bigg|_{x=0}=\lim_{N\to\infty}N[G(1)-g], \tag{9}$$

$$\frac{\partial^2 G}{\partial x^2}\bigg|_{x=0}=\lim_{N\to\infty}N^2[G(2)-2G(1)+G]. \tag{10}$$

To find the Green's function in lowest order of the concentration, we only need to take into account the perturbation caused by one impurity. For the contribution quadratic in the concentration we need the result of a pair of impurities, and so on.

The general method to obtain the Green's functions using a diagram technique is well known. The rules that apply for the calculations of the contributions from different diagrams in the case of anharmonic perturbations have to be slightly modified when phonon momentum operators come into play. Entering and leaving phonon lines represent $g(P(\vec{q}j)B^\dagger(\vec{q}'j'),\omega)$ and $g(B(\vec{q}j)P^\dagger\vec{q}'j',\omega)$. A complication arises when one wants to sum the contributions from all different diagrams because the diagrams can contain two perturbation terms in any number and order. It is therefore important that a phonon-momentum perturbation of the form (4) can be replaced by

$$T=-\frac{\hbar\omega^2}{4N}\left(\frac{M'}{M_0}-1\right)\sum_{\vec{q}j}\sum_{\vec{q}'j'}[\omega(\vec{q}j)\,\omega(\vec{q}'j')]^{-1/2}\times T(\vec{q}j,\vec{q}'j')B^\dagger(\vec{q}j)B(\vec{q}'j') \tag{11}$$

without changing the value of the disturbed Green's function. The complete perturbation can be written in phonon displacement operators. For one impurity,

$$H(1)=V(1)+T(1)=\frac{\hbar}{4N}\sum_{\vec{q}j}\sum_{\vec{q}'j'}[\omega(\vec{q}j)\,\omega(\vec{q}'j')]^{-1/2}\times Z(\vec{q}j,\vec{q}'j')e^{i(\vec{q}-\vec{q}')\cdot\vec{r}(s)}B^\dagger(\vec{q}j)B(\vec{q}'j'), \tag{12}$$

$$Z(\vec{q}j,\vec{q}'j')=-(M'/M_0-1)\,\omega^2\sum_{\alpha} w_\alpha^*(0\,|\vec{q}j)\times w_\alpha(0\,|\vec{q}'j')+D(\vec{q}j,\vec{q}'j'). \tag{13}$$

Z transformed into crystal space is the change in the dynamical matrix upon introduction of an impurity at lattice site (0, 0). The contribution of all scattering processes on one single impurity can now be found by collecting the terms for each value of n (Fig. 4) and summing the series thus obtained:

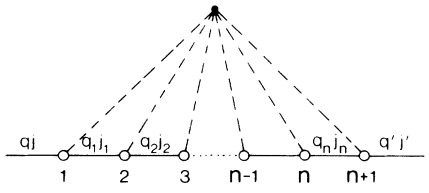

FIG. 4. Perturbation diagram with $n+1$ vertices. The broken lines indicate that all the perturbation vertices stem from one impurity only.

$$\left.\frac{\partial G}{\partial x}\right|_{x=0} = -\delta_{qq'}\frac{2kT}{\hbar}\frac{[\omega(\vec{q}j)\,\omega(\vec{q}j')]^{1/2}}{[\omega^2(\vec{q}j)-\omega^2][\omega^2(\vec{q}j')-\omega^2]} \times [Z(I+\Psi Z)^{-1}](\vec{q}j,\vec{q}j'), \quad (14)$$

where

$$\Psi(\vec{q}j,\vec{q}j') = \frac{\hbar}{2NkT\omega(\vec{q}j)}\,g(\vec{q}j,\omega)\,\delta_{qq'}\,\delta_{jj'}$$

and I is the unit matrix. Introduction of this result in Eq. (2) gives the contribution to the absorption coefficient.

This first-order effect gives us the local modes, gap modes, and induced absorption in the low-concentration limit at all the frequencies for which $Z(I+\Psi Z)^{-1}$ has a pole. The same results have been obtained before by simpler methods.

However, the second-order contributions can now be found in a way analogous to the first-order treatment. The perturbation can be written as

$$H(2) = \frac{\hbar}{4N}\sum_{\vec{q}j''}\sum_{\vec{q}'j'}[\omega(\vec{q}j)\,\omega(\vec{q}'j')]^{-1/2} \times Z(\vec{q}j,\vec{q}'j')\,(e^{i(\vec{q}'-\vec{q})\cdot\vec{r}(s)}+e^{i(\vec{q}'-\vec{q})\cdot\vec{r}(t)}) \times B^{\dagger}(\vec{q}j)\,B(\vec{q}'j') \quad . \quad (15)$$

The two impurities are at sites $(s,0)$ and $(t,0)$. The perturbation is the sum of two one-impurity perturbations and diagrams will consist of vertices from both impurities (Fig. 5). There are two infinite sets of contributions to $G(2)-g$ which originate from one of the impurities only. One such set is drawn as a sum of diagrams (Fig. 6), the values of the sum being represented by the left-hand symbol. Evidently this sum yields $G(1)-g$. Subtracting all the contributions from only one impurity, we obtain $G(2)-2G(1)+g$.

Now we have to add diagrams like Figs. 5(c) and 5(d), and these can be collected in the series of Fig. 7. We can also make such a series starting with the first vertex from the lower impurity. This will yield the same result as the one drawn in Fig. 7, and so we find that the contribution of Fig. 7, when multiplied by N^2, just equals

$$\left.\frac{1}{2}\frac{\partial^2 G}{\partial x^2}\right|_{x=0} .$$

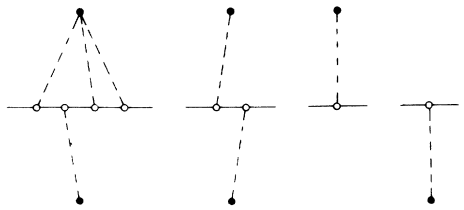

FIG. 5. Simplest two-impurity diagrams.

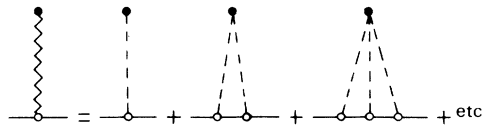

FIG. 6. Infinite set of contributions originating from one impurity only.

The contribution to $G(\mathrm{TOTO},\omega)$ becomes

$$-\frac{2NkT\omega_{\mathrm{TO}}}{\hbar(\omega_{\mathrm{TO}}^2-\omega^2)^2}(SP^{\dagger}S-SP^{\dagger}SPS+SP^{\dagger}SPSP^{\dagger}S-\cdots), \quad (16)$$

where $S=Z(I+\Psi Z)^{-1}$ is the result of the summation in Fig. 5, and $P(h)=\Psi e^{i\vec{q}\cdot\vec{r}(h)}$, $\vec{r}(h)=\vec{r}(t)-\vec{r}(s)$.

Denoting the series in Eq. (16) by $T(h)$, we can find

$$T(h) = SP^{\dagger}S - SP^{\dagger}T(-h) \quad . \quad (17)$$

From a purely mathematical point of view, we have solved the problem. We have converted an infinite series into an expression which can be evaluated by matrix inversion, and this inversion can be carried out in crystal space again. When one wants to do the actual calculations, difficulties arise because, first of all, the matrices involved in the inversion are complicated, and numerical evaluation will become lengthy, and secondly, the symmetry of the problem is reduced to the point group of the vector $\vec{r}(h)$ in the host crystal surroundings. However, Eq. (16) must still be averaged over all impurity pair configurations. All configurations that are symmetrically equivalent under the point-group elements of the host crystal must have equal probability. Hence their contributions have the same weight factor and can be summed as

$$T^0(h) = (d/l)\sum_R T(Rh) \quad (18)$$

where R denotes any point-symmetry element of the host crystal, d the number of equivalent configurations, and l the number of point-group elements. Applying (17) we obtain

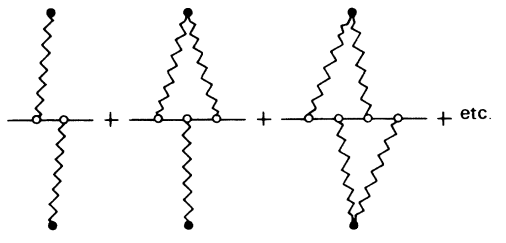

FIG. 7. Collection of infinite sets.

$$\sum_R T(Rh) = S\left(\sum_R P^{\dagger}(Rh)\right) S - S\sum_R P(Rh)\, T(Rh) \quad , \qquad (19)$$

which to a first approximation reduces to

$$T^0 = d\, SQS - SQT^0 \quad ,$$

where

$$Q = (1/l)\sum_R P^{\dagger}(Rh) \quad ,$$

and we can write

$$T^0 = d\,[I + SQ]^{-1} SQS \quad . \qquad (20)$$

This expression can be calculated with much less trouble, especially since it has the symmetry of the full point group of the host crystal. It must be carried to crystal space, where

$$Q_{\alpha\beta}\begin{pmatrix} l & l' \\ k & k' \end{pmatrix} = \frac{1}{Nl}\sum_{\vec{q}j} \frac{w_\alpha(k|\vec{q}j) w_\beta^*(k'|qj)}{\omega^2(\vec{q}j) - \omega^2} \times e^{i\vec{q}\cdot[\vec{r}(lk) - \vec{r}(l'k')]} \sum_R e^{i\vec{q}\cdot\vec{r}(Rh)} \quad . \qquad (21)$$

The second-order term of the optical absorption coefficient can now be built up from contributions of symmetrically inequivalent impurity configurations. Addition of the first-order term obtained from Eq. (14) gives the absorption coefficient, which will be compared with experiment in the next section. The second-order contribution has a striking analogy with the first-order term. The solutions of $\det[I + \Psi Z] = 0$ for the first order and of $\det[I + SQ] = 0$ for the second-order govern the contribution to the absorption coefficient. They are in one-to-one correspondence with the eigenfrequencies of the pure crystal. We expect, therefore, in both orders a reflection of the density of states of the host crystal, though much more hidden for the second order due to the more complicated weight factor.

RESULTS AND DISCUSSIONS

The Green's functions involved in the calculation have poles at the eigenfrequencies of the host lattice, so they will be complex. The imaginary part consists of the residues at these poles. The imaginary part is a weighted density of states and can be found as a histogram. The real part of the Green's function could be calculated by applying a Kramers-Kronig transformation.[17] We have chosen here a method in which the frequency is given a finite imaginary part Δ. This means that the residues at the poles, which have a δ-function shape are represented by Lorentzians, the width of which is determined by the value of Δ. Too small a value of Δ will cause spurious fluctuations in the Green's functions, while large values will smooth out essential details. We choose the optimum value for the imaginary part of the frequency by comparing the calculated density of states with several values of Δ, with the density of states obtained by making a histogram using 48 009 024 eigenfrequencies in the first Brillouin zone.[18] The matrix inversions involved in Eqs. (14) and (20) were carried out by the exchange step method.[19]

We could now calculate the impurity induced absorption for finite impurity concentrations, and compare the result with measured absorption spectra.

For the gap modes of low concentrations of Rb^+ in KI where the integrated absorption coefficient is a linear function of the impurity concentration one needs only to consider the perturbation term due to one impurity. Methods to be used in this case and results for different impurities have been given before.[20,21] An important point is that as the interparticle force constants are changed by the introduction of an impurity the lattice must relax around the impurity. The new interparticle distance then appears in the repulsive potentials. It has been shown by Bäuerle and Hübner[20] that this effect may not only affect the force constants between the impurity and its nearest neighbors, but also the force constants between the impurity and the more outward shells of ions. Inclusion of the lattice relaxation in an extended region around the impurity increases the complexity of the model, and the great number of adjustable parameters makes it difficult to draw conclusions from a comparison with experimental observations. Fortunately, a consideration of an extension of the lattice relaxation beyond the nearest neighbors does not seem necessary for the substitution of a Rb^+ ion in the KI lattice. Assuming the central force constant to be of Born-Mayer shape $A = (\lambda/\rho^2)\, e^{-r/\rho}$, we inserted for λ and ρ the values as they are for RbI. This should take into account the different electronic structure around the defect. The interionic distance between the impurity and its six nearest neighbors was then introduced as the only variable parameter. This model, which we believe to contain the essential features of an impurity in a host lattice, can now readily be compared with experiment. The gap mode frequencies for the two isotopes ^{85}Rb and ^{87}Rb were calculated as a function of the lattice relaxation; the result is shown in Fig. 8. The two experimentally determined gap mode frequencies give exactly the same lattice relaxation of 0.035 Å. This check on consistency is a very strong support of the method used. In contradistinction to the intensity of the gap modes, the intensity of the acoustic spectrum of KI: Rb^+ is not a linear function of the impurity concentration as appears from Fig. 3. In the model calculations we therefore take into account the contributions of single impurities and of impurity pairs. The second-order term is a sum of contributions of all symmetrically inequivalent

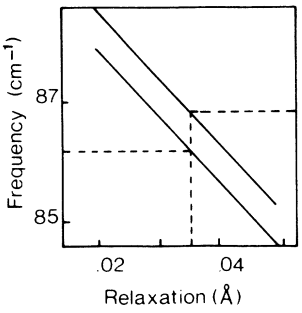

FIG. 8. Part of the calculated gap mode frequencies of $^{85}Rb^+$ (upper line) and $^{87}Rb^+$ (lower line) as a function of the lattice relaxation. The horizontally dashed lines give the experimentally formed values of the frequencies and the vertically dashed line the matching relaxation.

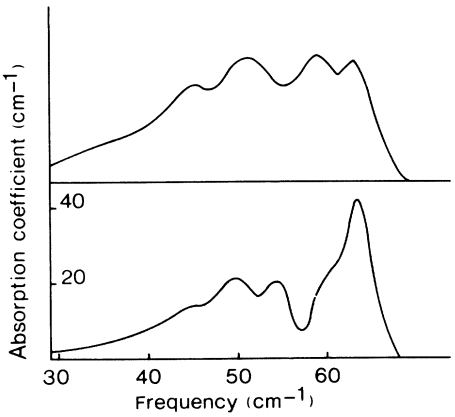

FIG. 10. Acoustic spectrum simulation of KI: Rb^+ with elastic relaxation fitting the gap modes (upper part) as compared with the experimentally determined spectrum.

two-impurity configurations. The magnitude of these contributions rapidly diminishes with increasing distance between the impurities. We therefore restricted the calculations to contributions from pairs of impurities neighboring in [110] directions and from pairs in [001] directions separated by one anion.

The first-order term is of course non-negative outside the TO frequency. However, the second-order term gives rise to positive as well as negative contributions. A negative second-order contribution means that intensity induced at a frequency by the first-order perturbation term is removed to another frequency by the second-order perturbation. Such negative contributions do explain the decline of the integrated intensity of the acoustic spectrum as a function of the Rb^+ concentration (Fig. 3). We calculated the first-order and second-order terms for several values of the elastic relaxation around the impurity. Then the contributions were added, choosing several values for the impurity concentrations. Figure 9 gives the result of the calculations in which we kept the host lattice undistorted, showing the concentration dependence of the simulated spectrum. With increasing elastic relaxation the intensity tends to shift to the high-frequency part of the spectrum. The value of the elastic relaxation that results from the gap mode calculation appears to give a reasonable fit for the acoustic spectrum as well (Fig. 10). Except for the details around 60 cm^{-1}, the agreement between the measured and the calculated spectrum is quite good.

This is a strong point in favor of the method used and seems to justify the assumptions made in this treatment. The main drawback of the method is the development of the quantities of interest in a Taylor series of the impurity concentration. At a certain instant the series will diverge; the question is at what concentration this will happen. In practice the limit will have to be set at an even lower concentration since the calculation of third- and higher-order terms will become too enormous a task. Although we neglected anharmonicity in view of the fact that the gap modes in the spectra are totally independent of the temperature between 5 and 20 K, one could easily include the anharmonic terms, which is a definite advantage of the method.

From our results on the system KI: Rb^+ we see that first- and second-order terms give a good description of the spectrum up to a concentration of a about 10 mole%. This leads us to the conclusion that the dielectric susceptibility of the mixed crystal exhibits continuous and moderate changes with increasing concentrations, and we infer that this also holds for the eigenfrequencies and eigenvectors. This result was to be expected for the eigenfrequencies since their shifts have to obey Rayleigh's theorem.

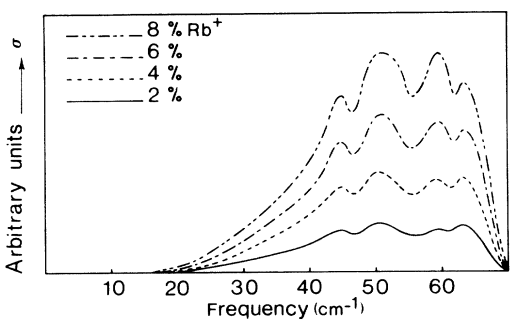

FIG. 9. Acoustic spectrum simulation of KI: Rb^+ without elastic relaxation for different concentrations.

ACKNOWLEDGMENTS

The authors are grateful to Dr. R. A. Cowley for providing us with the eigendata of KI. The work described here is part of the research program of the Foundation for Fundamental Research of Matter (FOM) and was made possible by financial support from the Netherlands Organization for Pure Research (ZWO).

[1]Th. Timusk and M. V. Klein, Phys. Rev. **141,** 664 (1966).
[2]K. F. Renk, Phys. Lett. **14,** 281 (1965).
[3]A. J. Sievers, A. A. Maradudin, and S. S. Jaswal, Phys. Rev. **138,** A272 (1965).
[4]I. G. Nolt, R. A. Westwig, R. W. Alexander, and A. J. Sievers, Phys. Rev. **157,** 730 (1967).
[5]B. P. Clayman, R. D. Kirby, and A. J. Sievers, Phys. Rev. B **3,** 1351 (1971).
[6]A. Mitsuishi, U. S.-Japan Cooperative Seminar On Far-Infrared Spectroscopy, 1965 (unpublished).
[7]H. W. Verleur and A. S. Barker, Phys. Rev. **164,** 1169 (1967)
[8]C. H. Perry and R. P. Lowndes, Quarterly Progress Report MIT No. 91, 1969 (unpublished).
[9]M. Iegems and G. L. Pearson, Phys. Rev. B **1,** 1576 (1970).
[10]R. D. Kirby, I. G. Nolt, R. W. Alexander, and A. J. Sievers, Phys. Rev. **168,** 1057 (1968).
[11]J. W. Cooley and J. W. Tukey, Math. Comput. **19,** 296 (1965).
[12]K. F. Renk, Z. Phys. **201,** 445 (1967).
[13]L. P. Kadanoff and G. Baym, *Quantum Statistical Mechanics* (Benjamin, New York, 1962).
[15]R. A. Cowley, *Phonons in Perfect Lattices and in Lattices with Point Inperfections* (Oliver and Boyd, London, 1966).
[16]P. S. Pershan and W. B. Lacina, Phys. Rev. **168,** 725 (1968).
[17]R. Metselaar and J. van der Elsken, Phys. Rev. **165,** 359 (1968).
[18]G. Dolling, R. A. Cowley, D. S. Schittenhelm, and I. M. Thorson, Phys. Rev. **147,** 577 (1966).
[19]E. L. Stiefel, *An Introduction to Numerical Mathematics* (Academic, New York, 1963).
[20]D. Bäuerle and R. Hübner, Phys. Rev. B **2,** 4252 (1970).
[21]C. de Jong, Solid State Commun. **9,** 527 (1971).